



Investigation of a haze-to-dust and dust swing process at a coastal city in northern China part I: Chemical composition and contributions of anthropogenic and natural sources



Wenqing Zhu^a, Yuxuan Qi^a, Huihui Tao^b, Haizhou Zhang^b, Wenshuai Li^a, Wenjun Qu^a, Jinhui Shi^c, Yingchen Liu^a, Lifang Sheng^a, Wencai Wang^a, Guanru Wu^a, Yunhui Zhao^a, Yanjing Zhang^a, Xiaohong Yao^c, Xinfeng Wang^d, Li Yi^a, Yingge Ma^e, Yang Zhou^{a,*}

^a Key Laboratory of Physical Oceanography/Collaborative Innovation Center of Marine Science and Technology, College of Oceanic and Atmospheric Sciences, Ocean University of China, Qingdao 266100, China

^b North China Sea Marine Forecasting Center of State Ocean Administration, Qingdao, Shandong, China

^c College of Environmental Science and Engineering, Ocean University of China, Qingdao, Shandong, China

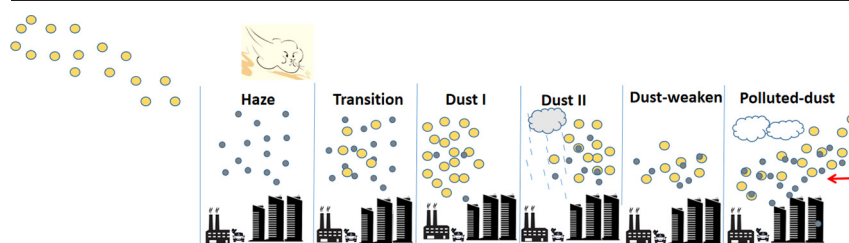
^d Environment Research Institute, Shandong University, Qingdao, Shandong, China

^e State Environmental Protection Key Laboratory of the Cause and Prevention of Urban Air Pollution Complex, Shanghai Academy of Environmental Science, Shanghai, China

HIGHLIGHTS

- A haze-to-dust event with a dust swing process was investigated in a coastal city.
- The dust swing process promoted the formation of sulfate.
- Local coal burning and waste incineration were the main contributors to haze.
- Secondary aerosol was transported to the site during the polluted dust period.

GRAPHICAL ABSTRACT



ARTICLE INFO

Editor: Jianmin Chen

Keywords:

Dust
PM_{2.5}
PM₁₀
Complex air pollution
PMF
PSCF

ABSTRACT

The long retention of dust air masses in polluted areas, especially in winter, may efficiently change the physicochemical properties of aerosols, causing additional health and ecological effects. A large-scale haze-to-dust weather event occurred in the North China Plain (NCP) region during the autumn-to-winter transition period in 2018, affecting the coastal city Qingdao several times between Nov. 27th and Dec. 1st. To study the evolution of the pollution process, we analyzed the chemical characteristics of PM_{2.5} and PM_{10-2.5} and source apportionments of PM_{2.5} and PM₁₀. The dust stagnated around NCP and moved out and back to the site, noted as dust swing process, promoting SO₄²⁻ formation in PM_{2.5} and NO₃⁻ formation in PM_{10-2.5}. Source apportionments were analyzed using the Positive Matrix Factorization (PMF) receptor model and weighted potential source contribution function (WPSCF). Before the dust invasion, Qingdao was influenced by severe haze; waste incineration and coal burning were the major contributors (~80%) to PM_{2.5}, and the source region was in the southwest of Shandong Province. During the initial dust event, mineral dust and the mixed factor of dust and sea salt were the major contributors (46.0% of PM_{2.5} and 86.5% of PM₁₀). During the polluted dust period, the contributions of regional transported biomass burning (22.3%), vehicle emissions (20.8%), and secondary aerosols (33.8%) to PM_{2.5} from the Beijing-Tianjin-Hebei region significantly increased. The secondary aerosols source was more regional than that of vehicle emissions and biomass burning and contributed considerably to PM₁₀ (30.8%) during the dust swing process. Our findings demonstrate that environmental managers should consider the possible adverse effects of winter dust on regional and local pollution.

* Corresponding author.

E-mail address: yangzhou@ouc.edu.cn (Y. Zhou).

1. Introduction

Complex regional air pollution is a common environmental issue in China, characterized by the combination of multiple air pollution processes (Aunan et al., 2018; Hu et al., 2015). Compared with their constituents in isolation, mixed pollutants in a complex pollution event may synergistically increase the harmful effects on the human body (Li et al., 2019). Complex pollution events often last for a few days, as a variety of natural and anthropogenic sources of particulate matter (PM) influence the pollution characteristics at different stages, altering the environmental and health impacts (Emberson et al., 2001; Fuzzi et al., 2017; Morishita et al., 2011; Xiao et al., 2013).

Previous research on haze and sand dust in China has focused on characterizing physicochemical properties of particulate matter and deriving the source apportionment information (Chan and Yao, 2008; Du et al., 2021; Fu et al., 2014; Nie et al., 2012; Shi et al., 2020). Haze and dust events in China typically have distinct synoptic conditions. Haze weather is prone to occur in winter, especially in the North China Plain (NCP) region, because of emissions from heating and poor atmospheric diffusion conditions (Wang et al., 2015), whereas dust days occur more frequently in spring because of Mongolian cyclones and/or Asian highs (Li et al., 2018; Pan et al., 2015; Zhang et al., 2003). However, more dust events have been observed recently in the transition period between autumn and winter (Wang et al., 2020b; Zhao et al., 2020a). According to our analysis of dust events from 2015 to 2018, three to eight Asian dust events affect the NCP region in late autumn and winter each year, and the average concentration of PM_{2.5} in NCP during dust events can be up to 39 $\mu\text{g m}^{-3}$ higher than non-dust days (Tables S1–S2).

The invasion of dust can further deteriorate the air quality in North China. On the one hand, mineral dust is a radioactively active aerosol that can absorb both short- and long-wave radiation (Chooari et al., 2014). Dust storms can perturb the temperature stratification, resulting in a warmer upper dust layer and lower surface temperature, making the planetary boundary layer more stable, indirectly aggravating local air pollution near the ground in eastern China (Wang et al., 2020b; Yang et al., 2021). On the other hand, dust usually has a large particle surface area where heterogeneous reactions that form secondary aerosols can occur (Zhang et al., 2018) or a photo-induced dust surface-mediated condensable vapor production (Nie et al., 2014). Moreover, the abundant transition metals in the mineral aerosol will catalyze the oxidation of SO₂, promoting the formation of sulfate (Cwiertyny et al., 2008; Li et al., 2020; Liu and Abbatt, 2021; Wang et al., 2021) and resulting in growth of particles (Nie et al., 2014). Above all, dust that occurs in the late autumn/winter may exacerbate environmental impacts due to the high primary emissions from heating and poor meteorological diffusion conditions (Beig et al., 2019; Cai et al., 2020; Oduber et al., 2019).

Recent studies on the complex events usually focused on the secondary formation of particles, revealing a more complex atmospheric chemistry process due to mixed pollutants, but few of them focus on the source apportionment variation of mixed pollution events (Dong et al., 2020; Huang et al., 2018; Ko et al., 2016; Wang et al., 2020a; Yang et al., 2019). As the formation mechanism and source are inseparable, identifying the variety of sources during the pollution evolution is critical to understanding their impact on the formation mechanism (Cesari et al., 2018; He et al., 2012). However, few studies focus on the source apportionment variation of mixed pollution events. During the transition period from autumn to winter in 2018, a large-scale haze-to-dust event occurred in North China. The dust air mass was transported out and back to Qingdao (a typical coastal city adjacent to the Yellow Sea), noted as a dust swing process in this study. This study is divided into two parts. In this section, the synoptic conditions of the haze-to-dust and dust swing process are analyzed and the contributions of different anthropogenic and natural sources and their potential source locations are identified and discussed, which are critical to understanding the complex physical and chemical evolution processes in the atmosphere. In Section 2, we will investigate the formation of secondary ions and the interactions between secondary aerosol formation and transition element (e.g., Fe and Mn) dissolution during the dust swing process.

2. Materials and methods

2.1. Sampling and chemical analysis

The sampling site was on the rooftop of the Baguanshan Atmospheric Research Observatory (36.03°N, 120.20°E; 74 m above sea level) in Qingdao (Fig. S1). This site is located 500 m away from the coastline of the Yellow Sea and on the outflow of Asian dust (Hao et al., 2007). The campaign was conducted from Nov. 9th to Dec. 4th 2018 (Fig. S2).

PM_{2.5} and PM₁₀ were collected using four high-flow particulate matter samplers (TE-6070BLX, Tisch Environmental Co., Ltd., USA and TH-1000C II, Wuhan Tianhong Instrument Co., Ltd., China) on Whatman® #41 filters and Pall® quartz filters. The sampling time for a single sample was about 12 h under normal air quality, usually from 8:00 a.m. to 8:00 p.m., and 3–6 h at a higher frequency under haze or dust conditions. We collected 113 PM_{2.5} samples and 107 PM₁₀ samples during the observation period.

Element concentrations (Al, V, Cr, Mn, Fe, Ni, Co, Cu, Zn, Ga, As, Se, Rb, Cd, Cs, Ba, Pb) were measured in samples collected on the #41 filters via inductively coupled plasma-mass spectrometry (iCAP Qc, Thermo Fisher Scientific, Germany) (Bowie et al., 2010). For the samples collected on quartz filters, the major ions were measured by Dionex ICS-3000 Ion Chromatography, and OC and EC were measured using a Sunset OC/EC analyzer. The concentration of organic matter (OM) was calculated as 1.6 times the OC concentration (Kong et al., 2019).

The hourly concentrations of PM_{2.5}, PM₁₀, and the gas phase pollutants were downloaded from the national urban air quality real-time release platform of the China National Environmental Monitoring Centre (<https://quotssoft.net/air/>). Hourly meteorological parameters, including the wind speed and direction and geopotential height, were derived from ERA5, the fifth-generation reanalysis data set published by the European Centre for Medium-Range Weather Forecasts (<https://cds.climate.copernicus.eu/cdsapp#!/dataset/reanalysis-era5-pressure-levels?tab=overview>).

2.2. Positive matrix factorization model

We used a positive matrix factorization (PMF) receptor model to analyze the sources of PM_{2.5} and PM₁₀ (Sowlat et al., 2016; Zhang et al., 2009). The PMF receptor model performs the optimal weighted least-squares fitting and can generate the minimum variance factor and accurately calculate the error estimate to improve stability (Tapper, 1993). PMF is widely used for atmospheric particulate matter source analyses (Lee et al., 2008; Pandolfi et al., 2011; Reff et al., 2007; Wang et al., 2019). Details of the conduction of PMF in this study can refer to Text S1 in the supporting information.

2.3. Backward trajectories and weighted potential source contribution function analysis

The backward trajectories during the sampling period was calculated by Hybrid Single-Particle Lagrangian Integrated Trajectory (HYSPPLIT4) model (<https://ready.arl.noaa.gov/hypub-bin/trajtype.pl?runtype=archive>) (Draxler and Rolph, 2010; McGowan and Clark, 2008). The hourly trajectories were computed backward for 72-h from the sampling site at 300 m above the ground surface. Meteorological data used in the HYSPLIT model was from the US National Center for Environmental Prediction Global Data Assimilation System (GDAS) with a resolution of 1.0 × 1.0° (Hersbach et al., 2020).

The potential source contribution function (PSCF), which is essentially a conditional probability function, is used to preliminarily determine the source area of pollutants (Pongkiatkul and Oanh, 2007; Zeng and Hopke, 1989; Zong et al., 2018). PSCF values were calculated from the 72-h backward trajectories and the concentration of the factor resolved by PMF (Wang, 2019). The calculated domain for PSCF was a range of 30–55°N, 75–125°E, and a grid cell with a resolution of 0.5° × 0.5° was divided (Kong et al., 2020). The weight potential source contribution function (WPSCF) was used in this study to reduce the uncertainty

(Dimitriou et al., 2020; Kulshrestha et al., 2009; Zhang et al., 2015). Details of PSCF and WPSCF can refer to Text S2 in the supporting information.

3. Results and discussion

3.1. Synoptic conditions of the haze-to-dust case

A regional haze event occurred in the NCP region from Nov. 24th to 26th, 2018, followed by a dust invasion from Mongolia (Tang et al., 2020; Zhao et al., 2020a). To understand the changes in the chemical characteristics of aerosols when the dust air mass mixed with local anthropogenic pollutants, we examined the haze-to-dust pollution episode at Qingdao from Nov. 27th to Dec. 1st. The episode was divided into six stages according to the meteorological condition and particle mass and compositions (Fig. 1), including the haze period (6:00–14:00 Nov. 27th), the transition period, in which a mixed sample was affected by both haze and dust (M; 14:00–18:00 Nov. 27th), dust I (DI; 18:00 Nov. 27th–00:00 Nov. 29th), dust II (DII; 0:00–17:00 Nov. 29th), dust-weakening (DW; 17:00 Nov. 29th–22:00 Nov. 30th), and polluted dust (PD; 22:00 Nov. 30th–21:00 Dec. 1st).

In Qingdao, haze occurred from 6:00 to 15:00 on Nov. 27th, with $PM_{2.5}$ concentrations ranging from $112 \mu\text{g}\cdot\text{m}^{-3}$ to $151 \mu\text{g}\cdot\text{m}^{-3}$, reaching moderate pollution levels as defined by the Chinese National Ambient Air Quality Standard (NAAQS, GB-3095-2012). The occurrence of haze was caused by stable weather conditions, e.g., a uniform pressure distribution, weak wind, and an inversion layer, as shown in Figs. 1, 2, and S3, respectively. According to the surface geopotential height and wind velocity colored with $PM_{2.5}$ concentrations in Fig. 2a–c, a transport of a high $PM_{2.5}$ concentration zone was observed from the Beijing–Tianjin–Hebei (BTH) region (marked by black circles) to the downwind NCP region, inducing the haze occurrence in Qingdao. In addition, the inversion layer on the morning of Nov. 27th resulted in poor dispersion conditions (Fig. S3), aggravating the haze pollution in Qingdao.

One sample was collected from 14:00 to 18:00 on Nov. 27th with an increase in PM_{10} concentration and a simultaneous decrease in $PM_{2.5}$ concentration (Fig. 1). During this period, the wind speed increased and the relative humidity (RH) declined rapidly in Qingdao, suggesting the site began being affected by the dry dust airflow (Fig. 2f). Thus this sample was collected during the transition period from haze to dust, influenced by both haze and dust pollution. This sample, noted mix (M) sample, revealed a decrease of $PM_{2.5}/PM_{10}$ from 0.57 in the haze period to 0.23 when the dust air mass arrived.

The distribution of PM_{10} concentration (Fig. 2d–f) shows that the dust plume appeared in Inner Mongolia on Nov. 26th and moved to the southeast (Fig. S4). The NCP region was gradually affected by the dust plume, and the dust air mass began to affect Qingdao at 14:00 on Nov. 27th (Fig. 2f). The PM_{10} concentration peaked at $671 \mu\text{g}\cdot\text{m}^{-3}$ at 00:00 on Nov. 28th. Till 00:00 on Nov. 29th, the dust plume continued to affect the NCP region (Fig. 2g). This period was defined as Dust I period (DI). A much lower average ratio of $PM_{2.5}/PM_{10}$ was observed in the DI period (0.11) than in the haze (0.57) and transition (0.36) periods.

At 00:00 on Nov. 29th, short-term precipitation occurred in Qingdao, accompanied by the movement of the dust plume and a significant decline in $PM_{2.5}$ and PM_{10} concentrations (Fig. 1). Because the dust plume stagnated in the NCP region, Qingdao was affected by dust air masses immediately after the rainfall, leading to a second increase in the $PM_{2.5}$ and PM_{10} concentrations (Fig. 2g–h). The ratio of $PM_{2.5}/PM_{10}$ was still below 0.25 from 1:00 to 18:00 on Nov. 29th. This period was named the Dust II episode (DII), during which Qingdao was affected by the stagnant dust air mass.

The dust plume moved slowly to the southwest under the easterly flow since 22:00 on Nov. 29th, and moved out of Qingdao (Fig. 2i). Under the influence of clean airflow from the Yellow Sea, the PM_{10} and $PM_{2.5}$ concentrations dropped from 160 and $34 \mu\text{g}\cdot\text{m}^{-3}$ to 89 and $15 \mu\text{g}\cdot\text{m}^{-3}$ defined as the Dust Weaken period (DW).

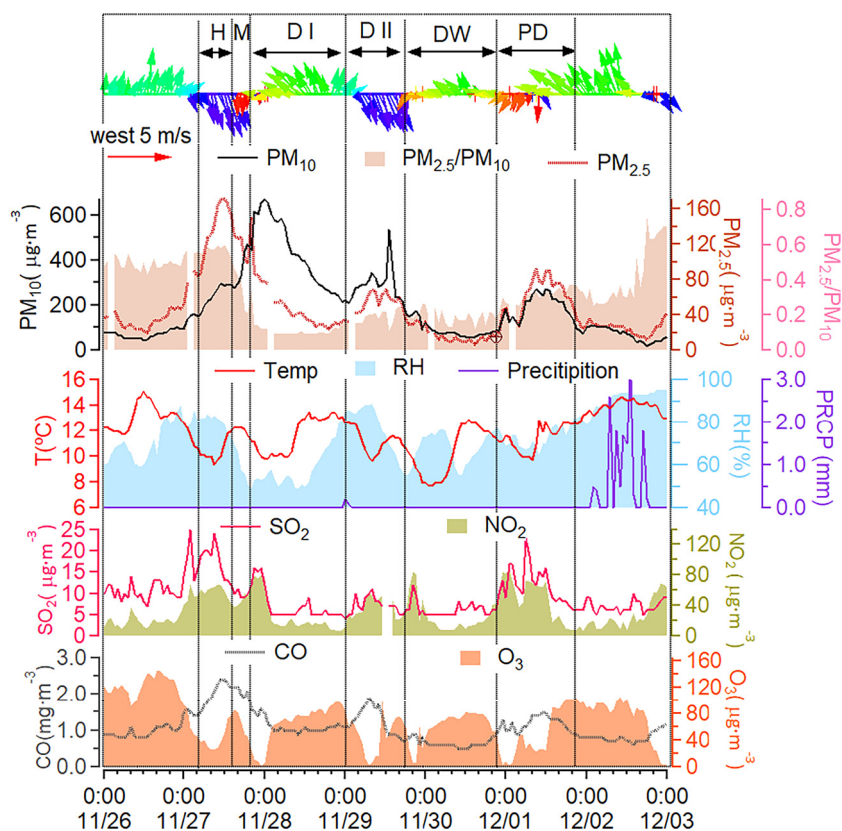


Fig. 1. Time series of meteorological parameters and mass concentrations of air pollutants during the haze-to-dust and dust swing process. H, M, DI, DII, DW, and PD stand for haze pollution, the transition period, in which a mixed sample was affected by both haze and dust, dust I, dust II, dust-weakening, and polluted dust periods. The time labels refer to China Standard Time (CST = GMT + 08:00).

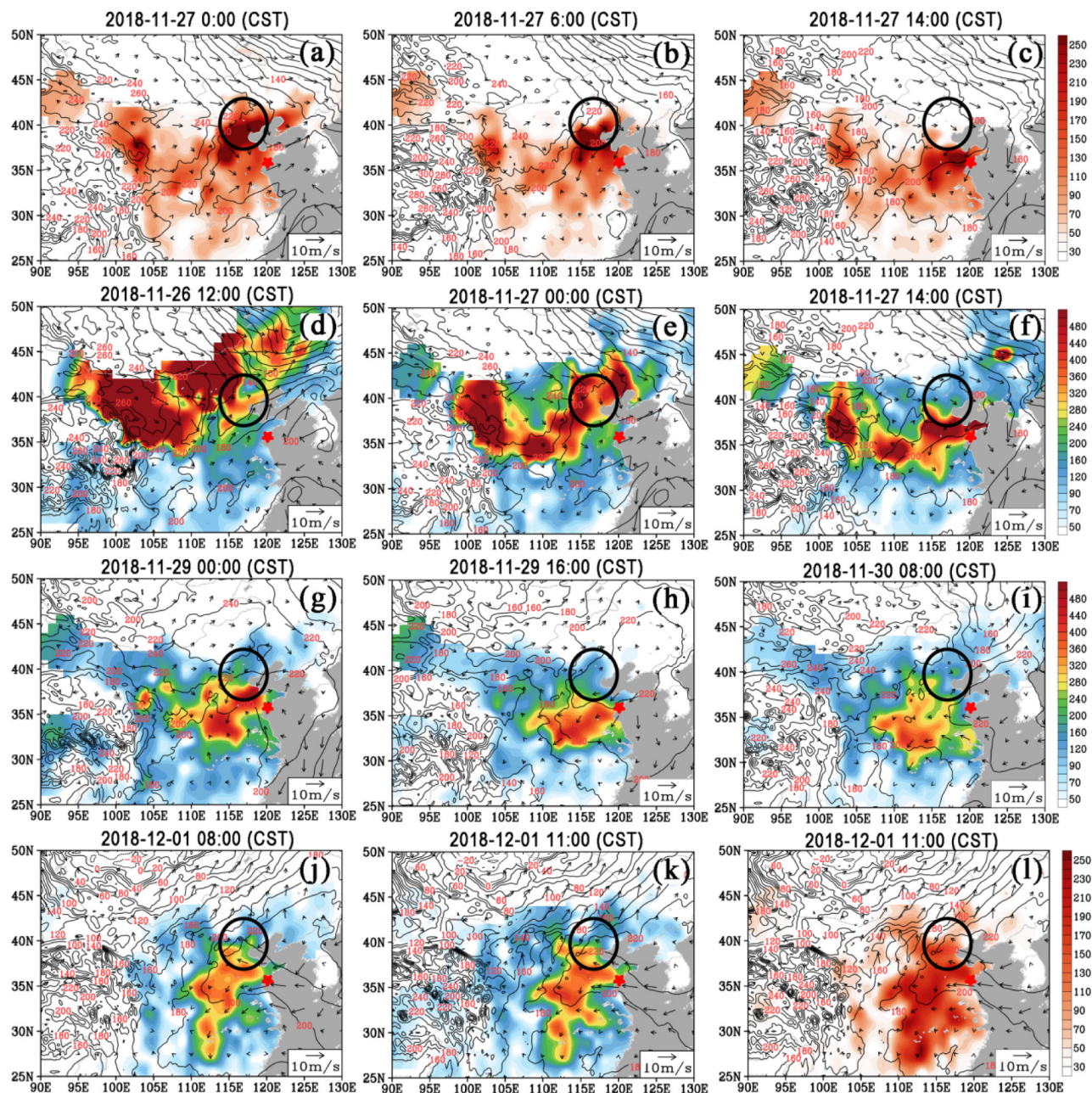


Fig. 2. The synoptic conditions at 1000 hPa and the mass concentrations ($\mu\text{g}\cdot\text{m}^{-3}$) of $\text{PM}_{2.5}$ (a–c, l) and PM_{10} (d–k) in the surface layer from Nov. 26th to Dec. 1st China Standard Time (CST). The black curves and vectors represent the geopotential heights (unit: gpm) at 1000 hPa with 20 gpm intervals and the wind velocity (unit: m/s). The Cressman interpolation method describes the horizontal distributions of the $\text{PM}_{2.5}$ and PM_{10} concentrations. The Beijing–Tianjin–Hebei region and Qingdao are marked by a black circle and a red star.

However, a swing of the dust air mass occurred in the NCP region (Fig. 2j–k). Since 8:00 on Dec. 1st, the dust air mass was slowly transported back to Qingdao by a southeastward wind. Unlike the previous two dust episodes, there was a wide range of high $\text{PM}_{2.5}$ concentration areas in the NCP region (Fig. 2l). As shown in Fig. 1, the $\text{PM}_{2.5}$ and PM_{10} concentrations in Qingdao increased during 4:00–16:00 on Dec. 1st, and the PM_{10} concentration was $>150 \mu\text{g}\cdot\text{m}^{-3}$ (Fig. 1). Considering that the average $\text{PM}_{2.5}/\text{PM}_{10}$ ratio during this period (0.31) was still lower than 0.4, we noted it as the Polluted Dust period (PD) (Guan et al., 2017; Li et al., 2018). As the dust air mass stayed and swung in the NCP region for four days, the complex pollution may have been affected by multiple chemical reactions and various sources because of mixing mineral aerosols with the regional/local emitted pollutants.

3.2. Component analysis during the haze-to-dust and dust swing process

The relative contributions and concentrations of the major components are displayed in Figs. 3 and S5, respectively. Given the low contributions from individual metals, we show the sum contributions in Fig. 3 and the details for each species in Fig. S6. Unfortunately, the ion data for PM_{10} were unavailable during the haze, transition, and DII periods due to instrument maintenance. As the haze event progressed, we observed significant increases in the concentrations of NO_3^- (from $21.48 \mu\text{g}\cdot\text{m}^{-3}$ to $32.77 \mu\text{g}\cdot\text{m}^{-3}$) and OM (from $19.04 \mu\text{g}\cdot\text{m}^{-3}$ to $40.95 \mu\text{g}\cdot\text{m}^{-3}$), accounting for 31.8 % and 39.7 % of the $\text{PM}_{2.5}$ concentration on average, respectively. Similar high contributions of NO_3^- and OM during the haze period were also observed in other cities in North China, suggesting that heterogeneous reactions may promote the

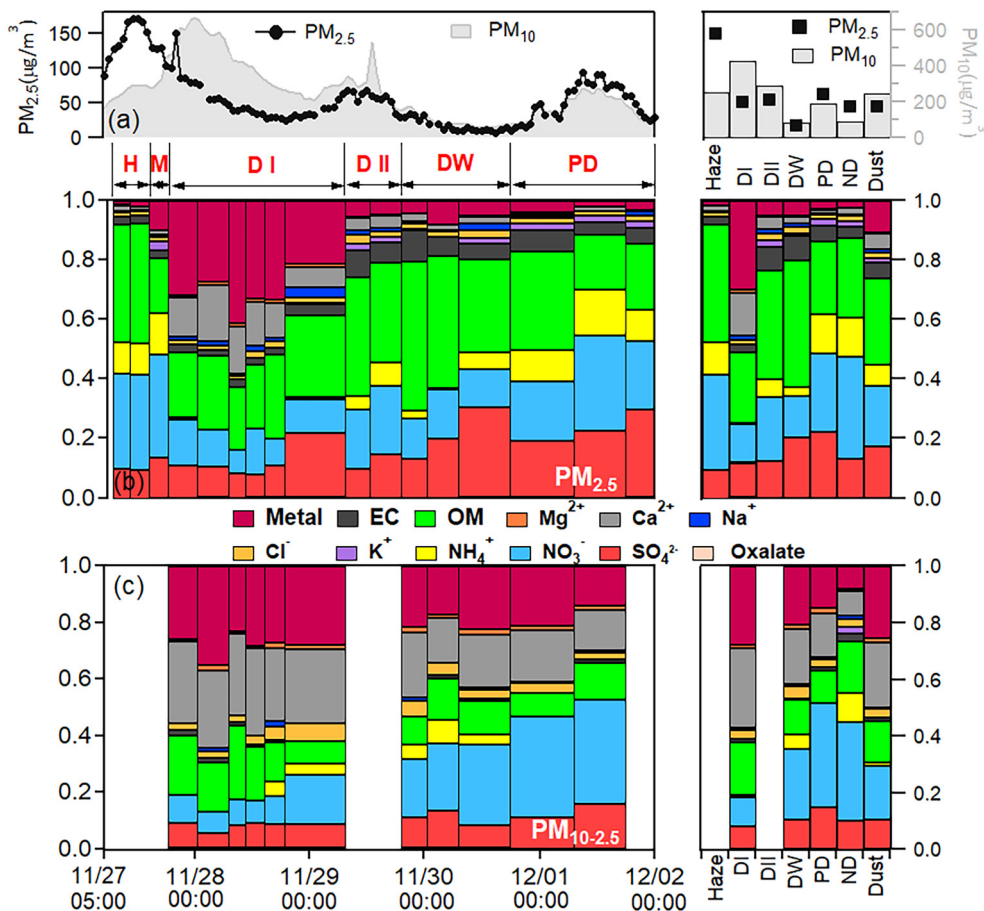


Fig. 3. Time series of (a) PM concentrations and the relative proportions of chemical compositions in (b) $PM_{2.5}$ and (c) $PM_{10-2.5}$ during the haze-to-dust and dust swing process. The right figures show the average ratios of the relative fractions of the components in $PM_{2.5}$ and PM_{10} during these periods. The abbreviations are the same in Fig. 1.

formation of secondary aerosols under high relative humidity (Cheng et al., 2015; Yang et al., 2015). Some metallic elements, including typical anthropogenic elements Cu, Zn, Pb, As, and Se, contributed 31.2 % of the total metals in the haze period but only 0.8 % during the DI period (Fig. S6).

When the dust invaded Qingdao, a mixed sample (M, Fig. 3) was collected during the transition period, influenced by haze and dust. The relative contribution of OM decreased sharply in $PM_{2.5}$ compared with the haze period. At the same time, the contribution of mineral elements increased under the dust effect. Among these elements, the relative contribution of typical crustal element Al increased (Fig. S6), with Al concentrations substantially increasing from $0.29 \mu\text{g}\cdot\text{m}^{-3}$ to $9.33 \mu\text{g}\cdot\text{m}^{-3}$ in $PM_{2.5}$ (Fig. S7). In contrast, the concentrations of the anthropogenic pollutants Pb, Zn, Cd, and As in $PM_{2.5}$ significantly decreased (Fig. S7). Although the $PM_{2.5}$ concentration decreased, the SO_4^{2-} concentration in $PM_{2.5}$ increased from $10.14 \mu\text{g}\cdot\text{m}^{-3}$ to $15.45 \mu\text{g}\cdot\text{m}^{-3}$ and the contribution of SO_4^{2-} increased from 9.8 % to 13.1 %.

Compared to the mixed $PM_{2.5}$ sample (M), the $PM_{2.5}$ sample collected during the dust peak (the first sample of the DI period) contained more mineral elements and Ca^{2+} . The sum concentrations of Al, Fe, and Ca^{2+} increased to $84.67 \mu\text{g}\cdot\text{m}^{-3}$ in $PM_{10-2.5}$, more than four times that in $PM_{2.5}$ ($17.85 \mu\text{g}\cdot\text{m}^{-3}$). These three crustal species account for 43.2 % of $PM_{2.5}$ and 54.8 % of $PM_{10-2.5}$ during the DI period. Secondary species NO_3^- showed a more rapid decrease than SO_4^{2-} in both concentration and contribution in the DI period.

After the precipitation, the chemical composition of PM changed significantly during DII period. The contribution of mineral elements obviously decreased, while EC, NO_3^- , and NH_4^+ increased (Fig. 3). The backward trajectories during DII period showed that the airflow stagnated on the surface layer (under 900 hPa) of Qingdao for up to 50 h—nearly twice as long as

that in DI period (Fig. S8). Therefore, the aerosol collected during DII period was greatly affected by local emissions.

During the DW period, the concentrations and relative contributions of mineral elements in $PM_{2.5}$ continued to decrease (Figs. 3 and S5). The concentrations of SO_4^{2-} , NO_3^- and OM in $PM_{2.5}$ were 2–6 times lower than those in the DII period, but the relative contributions of these species increased (Fig. 3).

During the PD period, the contribution of mineral elements in $PM_{2.5}$ (2.5 %) was higher than that during the non-dust period (1.8 %). We also observed higher Al and Fe concentrations in $PM_{10-2.5}$ (Fig. S6). Unlike DI and DII, the contribution of NH_4^+ increased to 13.1 % during the PD period, suggesting the influence of human activities (Murano et al., 1998; Park et al., 2018). According to the backward airflow trajectory, this PD period may be influenced by air masses transported from the BTH region (Fig. S9), where the concentrations of PM_{10} in Beijing and Tianjin were as high as 200 and $250 \mu\text{g}\cdot\text{m}^{-3}$, respectively. The transported air mass passed through the Bohai Sea and the Yellow Sea before arriving in Qingdao; thus, a consistently high RH (67–82 %) was observed during the PD period. This high RH may have induced the gradual increases in SO_4^{2-} concentrations in both $PM_{2.5}$ and $PM_{10-2.5}$ (Figs. 3 and S5).

Comparing the major components between $PM_{2.5}$ and $PM_{10-2.5}$ (Figs. 3 and S5), mostly OM and secondary ions, such as NO_3^- , SO_4^{2-} , and NH_4^+ , existed in $PM_{2.5}$, especially in the haze period, and more crustal compositions existed in $PM_{10-2.5}$. For the three dust periods, the sum of the mineral metals (Al, Fe, Cr, Mn, Co, Ba) and Ca^{2+} more substantially contributed to the $PM_{10-2.5}$ (29.2 %) than the $PM_{2.5}$ (9.9 %). The increase in mineral components combined with changes in the atmospheric environment may have impacted the formation of secondary aerosols. As shown in Fig. 3, the relative contribution of SO_4^{2-} in $PM_{2.5}$ increased as the dust event progressed.

The average contribution of SO_4^{2-} in $\text{PM}_{2.5}$ increased from 9.84 % in the haze period to 11.56 % in DI and 12.06 % in DII. Remarkably high sulfate contributions were observed during the DW (19.8 %) and PD (21.6 %) periods. Although the $\text{PM}_{10-2.5}$ data are incomplete, we also observed a higher contribution of SO_4^{2-} in $\text{PM}_{10-2.5}$ in DW (14.0 %) and PD (18.9 %) than in DI (8.7 %). This information indicates the production of SO_4^{2-} in both fine and coarse PM during the dust swing process. NO_3^- and NH_4^+ showed similar variations in $\text{PM}_{2.5}$, both of which are indicators of human activities (Lin et al., 2007; Murano et al., 1998; Park et al., 2018). The relative contributions of NO_3^- and NH_4^+ in $\text{PM}_{2.5}$ were lowest during the DI period and increased during DII and PD periods when the air masses were more influenced by the lower troposphere and air mass transport from the BTH region. NO_3^- in $\text{PM}_{10-2.5}$ showed similar trends, but more NO_3^- was produced in $\text{PM}_{10-2.5}$ than in $\text{PM}_{2.5}$. But NH_4^+ in $\text{PM}_{10-2.5}$ showed minimal contribution during the three dust periods because it is mainly concentrated in fine particles (Mace, 2003; Wang et al., 2003; Wang et al., 2014). Our detailed investigation of the secondary ions is discussed in Part II of this study.

3.3. Source analysis

3.3.1. The PMF factors

In this study, nine $\text{PM}_{2.5}$ and ten PM_{10} factors were finally identified (Fig. 4). The average contribution proportions in PM can be found in Fig. S10.

The main species defining factor 1 for $\text{PM}_{2.5}$ were NO_3^- , NH_4^+ , Zn, As, and Pb. Although we usually ascribe SO_4^{2-} and NO_3^- to the typical stationary source and moving source emissions, a recent isotope study suggested that coal burning is the dominant source of NO_3^- in Northeast China (Zhao et al., 2020b). As and Pb are elements commonly released from coal combustion, and Pb, Zn, and Cu are often observed in emissions from municipal solid waste incineration (Abanades et al., 2002; Li, 2004). Previous studies have shown that coal burning and waste incineration sources contain large amounts of Cl^- (Lucarelli et al., 2019; Park et al., 2019; Shang et al., 2019). Thus, factor 1 was identified as a mixed emission from coal burning and waste incineration. In PM_{10} , however, coal burning and waste incineration are identified as two factors and the coal-burning factor was characterized by a high proportion of As, a typical marker for coal-fired power plant emissions (Tan et al., 2015; Zhou et al., 2014). As shown in Fig. S11, several data were unavailable for PM_{10} in the period with the high contributions of coal burning & waste incineration during the haze pollution, which may cause the difference between $\text{PM}_{2.5}$ and PM_{10} .

The biomass burning factor had relatively high loadings of K^+ , consistent with previous reports (Yan et al., 2015; Zhang et al., 2010; Zong et al., 2016). Zn and Ba are also typical elements of biomass combustion (Li et al., 2007). The factor of secondary aerosols was characterized by high SO_4^{2-} and oxalate loadings, which are generally produced by secondary liquid phase reactions (Contini et al., 2010; Yu et al., 2005). The traffic

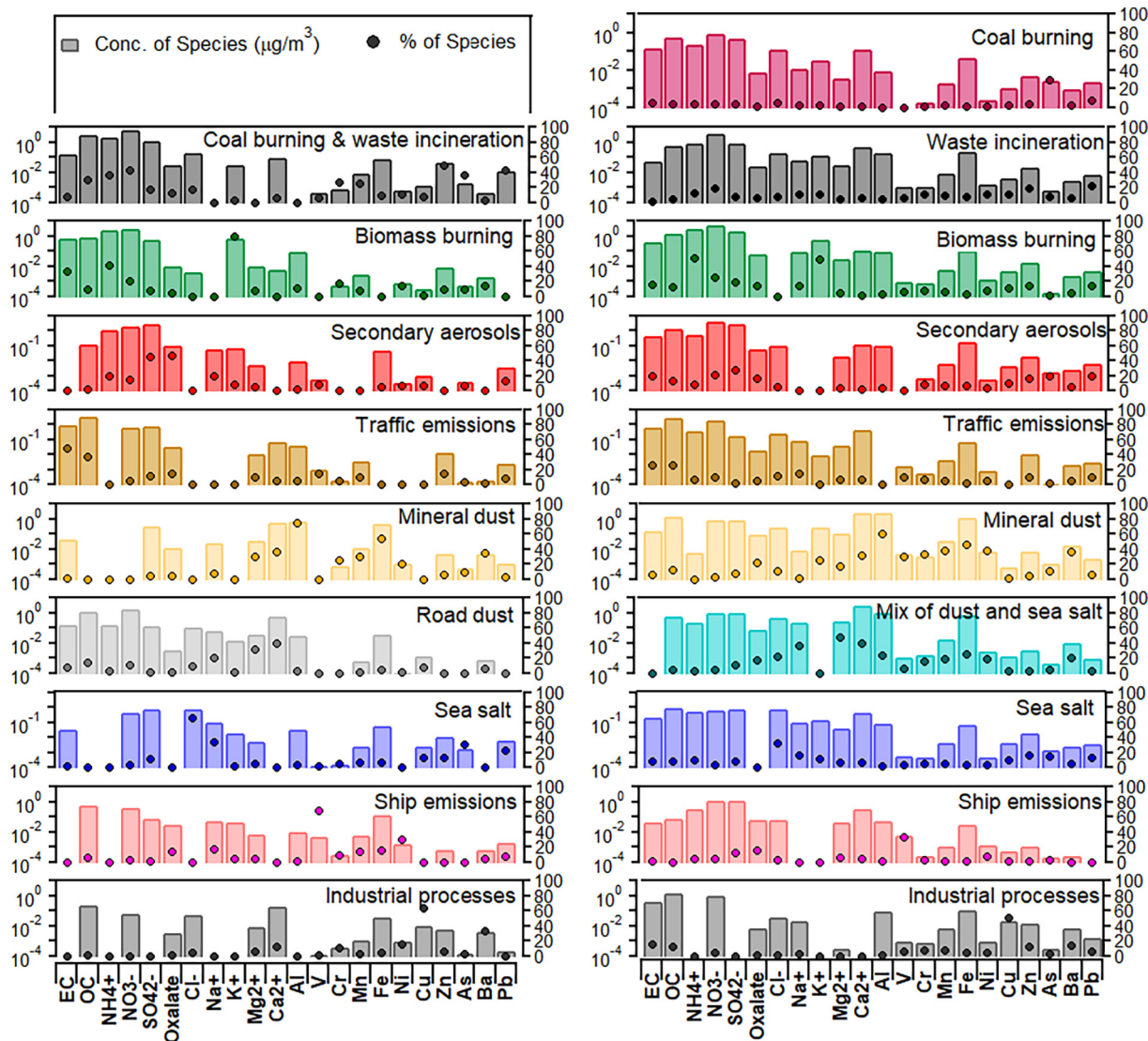


Fig. 4. The contribution profiles of nine factors of $\text{PM}_{2.5}$ and ten factors of PM_{10} identified by the PMF model.

emissions factor had high loadings of EC and OC, major pollutants from gasoline and diesel combustion (Liu et al., 2016; Liu et al., 2019). Zn also had a relatively high loading in this factor, which could be attributed to tire wear and lube oil additives (Begum et al., 2004; Fergusson and Kim, 1991).

The Mineral dust factor consisted of crustal dust elements, such as Al, Fe, Ba, and Mn (Bilos et al., 2001; Shi et al., 2009; Wu et al., 2020). The road dust factor in PM_{2.5} was identified by high loadings of Mg²⁺, Ca²⁺, EC, and OC and the moderate contributions of Cu and Ba. Mg²⁺ and Ca²⁺ mainly come from industrial emissions and construction activities (Han et al., 2007). EC and OC are released in vehicle emissions (Ke et al., 2008; Querol et al., 2013), and brake wear and tire friction can produce Cu (Lin et al., 2015). While in PM₁₀ there is a mixed factor of dust and sea salt, consisting of both crustal tracers, including Al, Fe, Mg²⁺, and Ca²⁺ (Koçak et al., 2011) and fresh sea salt aerosol ions, Na⁺ and Cl⁻ (Gupta et al., 2015). This factor showed high contributions during the DI period, which passed over the Bohai Sea before arriving at the site (Figs. S8 and S11).

Sea salt and ship emission were two marine source factors. The sea salt factor was characterized by abundant Na⁺ and Cl⁻ (Gupta et al., 2015; Park et al., 2019). The ship emission factor had high proportions of Ni and V, which are typically associated with emissions from residual oil, indicating that these species were likely derived from shipping activities and industrial processes (Pey et al., 2013).

The last factor was industrial processes, characterized by high loadings of Cu, Ba, and some Zn, Cr, and Ni (Amil et al., 2016; Soleimani et al., 2018). Previous studies have reported that metal melting plants are major sources of Cu, Zn, and Cr (Lee and Hieu, 2011; Liu et al., 2017), and power plants are major sources of Cr and Cu (Marcazzan et al., 2001; Schauer et al., 2002). Ba and Ni are released in industrial pollution from metal smelting (Font et al., 2022; Xiao et al., 2021).

3.3.2. Relative contributions of factors in the haze-to-dust and dust swing processes

The relative contributions and concentrations of each factor identified by PMF for PM_{2.5} and PM₁₀ are shown in Figs. 5 and S11. The coal burning

and waste incineration factor was the dominant source of PM_{2.5} during the haze episode, accounting for 79.1 %. Traffic emissions factor was the second highest one, which maybe because of the accumulation of local emissions, considering the poor dilution conditions.

For the mix samples (M) collected during the transition period, the contributions of biomass burning, secondary aerosols, and mineral dust in PM_{2.5} significantly increased to 30.7 %, 16.4 %, and 3.0 %, respectively (Fig. 5). These sources may have been partially transported from the BTH region. When Qingdao was affected by dust plumes (DI), the primary contributing source of particles was dust and a mix of dust and sea salt sources, which contributed 31.1 % of PM_{2.5} and 86.5 % of PM₁₀, respectively. Ship emissions accounted for 9.0 % of PM_{2.5} during DI because of the transport of airflow from the southwest passing over the Bohai Sea and the Yellow Sea (Fig. S8).

After the precipitation event, the contribution of mineral dust in PM_{2.5} was reduced to 6.5 % in DII, and the contributions of traffic emissions and biomass burning rose to 33.8 % and 23.1 %, respectively (Fig. 5). Changes in the source contributions demonstrated that the aerosol particles collected during DI were mainly contributed by mineral dust, whereas those collected during DII were more greatly affected by local emissions, which were proved by the backward trajectories (Fig. S8).

In the DW period, we can find the contributions of secondary aerosol, sea salt and ship emissions to PM_{2.5} were increasing (Fig. 5), under the control of the marine source air mass from the Yellow Sea (Fig. 2i). While the secondary aerosols and traffic emissions significantly increased in PM₁₀. In the PD period, the contributions from biomass burning, coal burning and waste incineration sources significantly increased in PM_{2.5} and the secondary aerosols dominated the source of PM₁₀ (50.3 %).

During the DI, DII, and PD periods, mineral dust aerosols contributed less to PM, and the contributions of secondary aerosols and traffic emissions substantially increased. The increase in the relative contribution of the secondary aerosol factor corresponds to the increase in the SO₂²⁻ concentration, which was probably promoted by the liquid-phase reaction. The vehicle

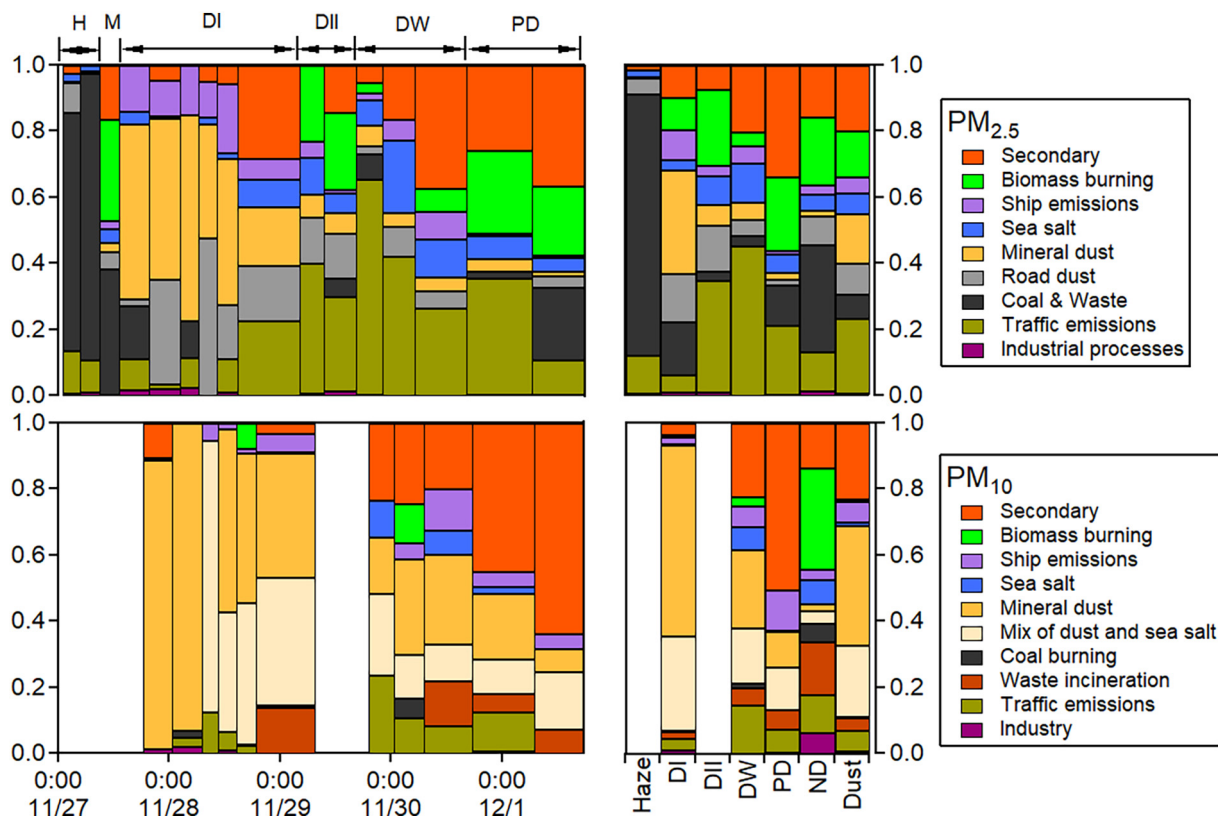


Fig. 5. The time series (left) and average (right) relative contributions of the source factors to (a) PM_{2.5} and (b) PM₁₀ during haze-to-dust and dust swing episodes. The abbreviations are the same in Fig. 1.

emissions, biomass burning, coal burning, and waste incineration sources, which accounted for significant proportions during the haze and PD periods, contributed more to $PM_{2.5}$. Mineral dust and the mixture of dust and sea salt sources, which accounted for large proportions during the DI period, contributed more to PM_{10} .

3.3.3. Regional sources of the contributing factors on the dust and non-dust days

The WPSCF was used to analyze the potential source distribution of the major factors contributing to PM to determine the regional transport characteristics of pollutants (Li et al., 2017). Because of the short occurrence time of the haze event, few paths could be used to calculate the WPSCF separately. Thus, we separated the sampling period into dust and non-dust periods for the WPSCF analysis to reduce uncertainty. The dust period comprised the DI, DII, DW, and PD days, and the non-dust period included all other sampling days, excluding the dust days. We plotted the backward trajectories during the haze period in red on the non-dust figures to find the impacts of haze on regional PM sources. A larger WPSCF indicates a more significant contribution of the regional sources to the pollutants at the receptor site (Ren et al., 2021). In this study, we considered areas with WPSCFs >0.7 as the areas with the most significant contribution to the pollutant (Zhang et al., 2015).

As shown in Fig. 6, during the dust period, the high WPSCFs of the major factors in $PM_{2.5}$ and PM_{10} can be classified into two distributions. The dust particles in both $PM_{2.5}$ and PM_{10} and the mixed source of dust and sea salt in PM_{10} mainly originated from long-range transport from Siberia and Mongolia that turned back toward the west after arriving at the Bohai Sea. Secondary aerosols, traffic emissions, biomass burning,

and coal burning and waste incineration in $PM_{2.5}$ were generally distributed in Shandong province and the Bohai Sea. The WPSCF distribution with lower values (<0.7) for biomass burning on dust days in PM_{10} indicates that biomass burning had a minor contribution to PM_{10} during the dust period. The transport paths for traffic emissions and secondary aerosols on dust days were from the BTH region for $PM_{2.5}$ and PM_{10} . Traffic emission sources were more locally derived compared with the secondary aerosols. The potential source distribution of the mineral dust and the mixed factor of dust and sea salt on dust days were distributed at sea. The mineral dust particles were mixed with sea salt particles to some extent when the dust air flow passed over the sea before reaching Qingdao during the dust period (Figs. S8 and S9). The average RH during these periods was not very low (68%), especially during the PD period (65–82%). When dust or aging dust particles are transported with gases to the marine boundary layer, secondary aerosols are produced, and the high RH of the marine environment can supply water content for heterogeneous reactions to occur. Thus the high WPSCF of the mineral dust factor in $PM_{2.5}$ and PM_{10} and the mixed factor of dust and sea salt in PM_{10} on the dust days were distributed at sea.

During non-dust days, most of the major contributing factors, including traffic emissions, biomass burning, coal burning and waste incineration, showed high loadings in the south of Shandong Province. The high WPSCF distributions of secondary aerosols were located in the Yangtze-Huaihe River Basin (indicated by a black block in Fig. 6) and near the coast of the Yellow Sea. The source regions of secondary aerosols in $PM_{2.5}$ are related to high RH (Huang et al., 2015). Generally, dust or mixed dust and sea salt during the non-dust period were not evident. As marked with

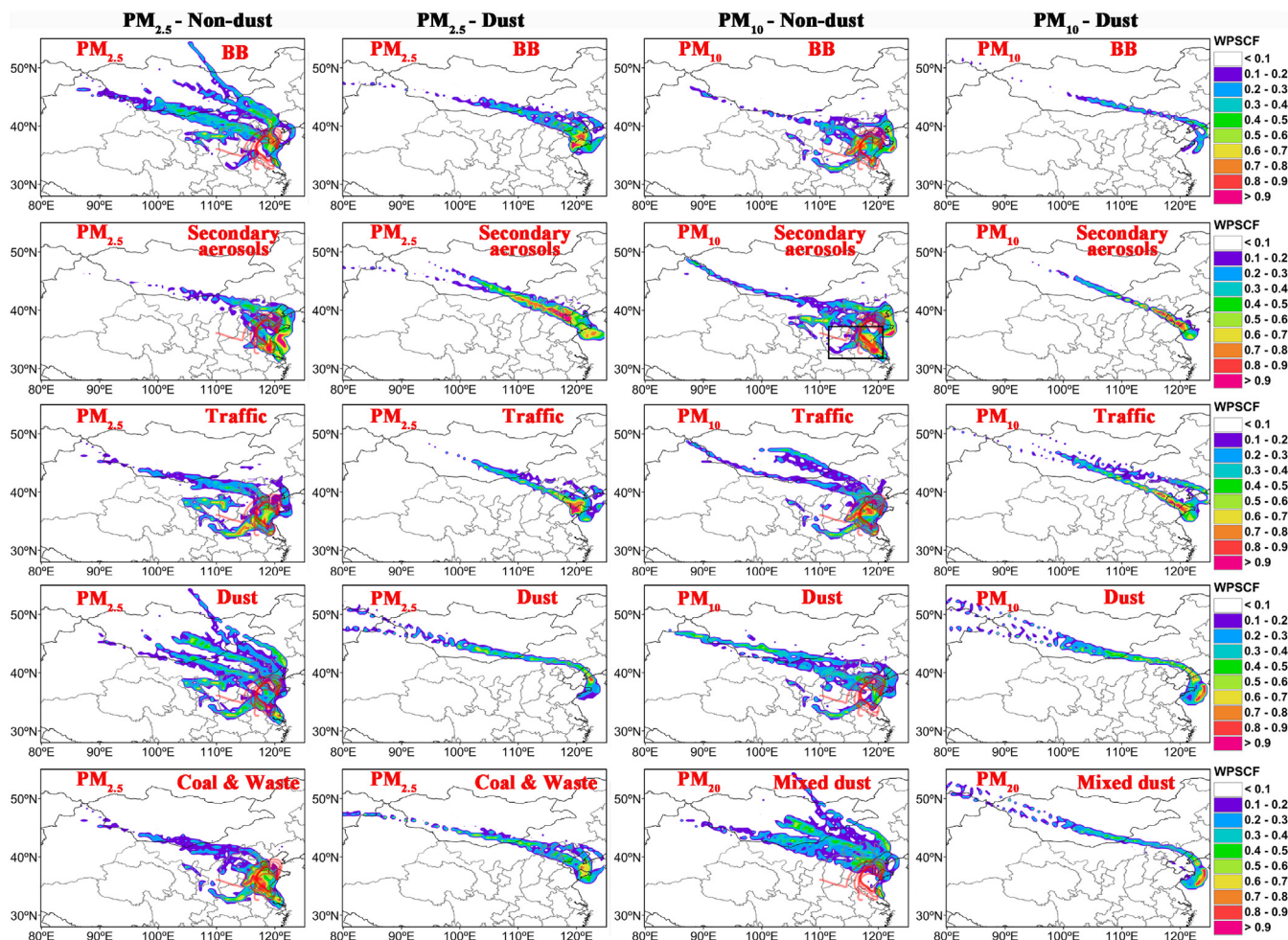


Fig. 6. The WPSCF distributions of the factors contributing to $PM_{2.5}$ and PM_{10} during the non-dust and dust periods. The red backward trajectories during the haze period are shown in the non-dust figures.

red lines in the non-dust period, the backward trajectories of the air mass during the haze period are mostly located in the high WPSCF areas of coal burning and waste incineration and traffic emissions. These two factors were the major contributors to PM_{2.5} during the haze period.

4. Conclusion

A long-lasting haze-to-dust and dust swing process (Nov. 27th–Dec. 1st) was investigated during the autumn/winter transition period in Qingdao, a coastal city in North China. Combined with the analysis of pollutant distribution and synoptic conditions, we found that haze pollution was influenced by the transport of polluted air masses from the BTH region. In addition, the south wind provided a warm and humid airflow to Qingdao with an inversion layer that resulted in poor dispersion, exacerbating the haze pollution. During the haze period, coal burning and waste incineration factors contributed nearly 80 % to PM_{2.5}.

The four-day dust pollution event was mainly due to the stagnation of the dust air mass in the NCP region. The dust plume slowly moved to the southwest under the easterly wind, moving out and then back to Qingdao. To investigate the pollution evolution, we divided the whole process into three different dust events with one dust-weaken period identified. The DI period was an intense dust event, with the highest concentrations of crustal metals (Al and Fe, and Ca²⁺), accounting for 43.2 % in PM_{2.5} and 54.8 % in PM_{10-2.5}. During this initial dust period, mineral dust, road dust, or the mixed factor of dust and sea salt were the dominant sources of PM_{2.5} (46.0 %) and PM₁₀ (86.5 %), respectively. According to the backward trajectories analysis, Qingdao was influenced more by the surface pollutant emissions as the dust stagnated (DII and PD periods), resulting in the mixing of the dust air mass with local pollutants during transport. We observed significant SO₄²⁻, NO₃⁻ and OM production in the PM_{2.5} and NO₃⁻ production in the PM₁₀. Biomass burning (23.1 %) and vehicle emissions (33.8 %) contributed considerably to PM_{2.5} in the DII period. During the PD period, secondary aerosols contributed most to PM_{2.5} (33.8 %) and PM₁₀ (56.7 %). In contrast, this factor only contributed 9.8 % and 3.6 % to PM_{2.5} and PM₁₀ in the DI period, indicating more aged dust in the PD period.

The potential contribution source regions of the PMF factors were analyzed via the WPSCF. During non-dust days, the high WPSCF of biomass burning, vehicle emissions, secondary aerosols, coal burning, and waste incineration were mainly distributed in the south of Shandong Province, where the airflow passes during haze. Mineral dust and the mixed factor of dust and sea salt were generally transported long-range from Siberia and Mongolia, turning west toward the site upon arrival at the Bohai Sea. From the WPSCF result during the dust days, biomass burning, vehicle emissions, and secondary aerosols in PM_{2.5} were transported from the BTH region to the site during the dust swing period. The WPSCF distribution suggests that the high potential sources of biomass burning and vehicle emissions were more local than that of secondary aerosols, which also contributed to PM₁₀.

CRedit authorship contribution statement

Wenqing Zhu: Formal analysis, Writing–original draft, Validation, Writing–review & editing. **Yang Zhou:** Conceptualization, Writing–review & editing, Validation, Funding acquisition, Supervision, Project administration. **Yuxuan Qi:** Investigation, Formal analysis, Validation. **Huihui Tao:** Methodology. **Haizhou Zhang:** Methodology. **Wenshuai Li:** Investigation, Formal analysis, Validation. **Wenjun Qu:** Methodology. **Jinhui Shi:** Writing–review & editing, Funding acquisition. **Yingchen Liu:** Investigation, Methodology. **Lifang Sheng:** Validation, Writing–review & editing. **Wencai Wang:** Validation, Writing–review & editing, Methodology, Funding acquisition. **Guanru Wu:** Investigation., Validation. **Yuanhui Zhao:** Investigation, Validation. **Yanjing Zhang:** Investigation, Validation. **Xiaohong Yao:** Validation, Methodology. **Xinfeng Wang:** Methodology. **Li Yi:** Methodology. **Yingge Ma:** Methodology.

Data availability

Data will be made available on request.

Declaration of competing interest

The authors declare that they have no known competing financial interests or personal relationships that could have appeared to influence the work reported in this paper.

Acknowledgments

This research was supported by the National Natural Science Foundation of China (Grant Numbers: 41875155, 41605114, 41876131, 41875174), the National Key Basic Research Project of China (2019YFA0607004). This study was also supported by the State Environmental Protection Key Laboratory of Formation and Prevention of Urban Air Pollution Complex. We are grateful to Shanhong Gao from the College of Oceanic and Atmospheric Sciences, Ocean University of China, for his support with the field campaign in Qingdao, China. The authors gratefully acknowledge the NOAA Air Resources Laboratory (ARL) for providing the HYSPLIT transport and dispersion model.

Appendix A. Supplementary data

Supplementary data to this article can be found online at <https://doi.org/10.1016/j.scitotenv.2022.158270>.

References

- Abanades, S., Flamant, G., Gagnepain, B., Gauthier, D., 2002. Fate of heavy metals during municipal solid waste incineration. *Waste Manag. Res.* 20, 55–68.
- Amil, N., Latif, M.T., Khan, M.F., Mohamad, M., 2016. Seasonal variability of PM 2.5 composition and sources in the Klang Valley urban-industrial environment. *Atmos. Chem. Phys.* 16, 5357–5381.
- Annan, K., Hansen, M.H., Wang, S., 2018. Introduction: air pollution in China. *China Q.* 234, 279–298.
- Begum, B.A., Kim, E., Biswas, S.K., Hopke, P.K., 2004. Investigation of sources of atmospheric aerosol at urban and semi-urban areas in Bangladesh. *Atmos. Environ.* 38, 3025–3038.
- Beig, G., Srinivas, R., Parkhi, N.S., Carmichael, G.R., Singh, S., Sahu, S.K., et al., 2019. Anatomy of the winter 2017 air quality emergency in Delhi. *Sci. Total Environ.* 681, 305–311.
- Bilos, C., Colombo, J.C., Skorupka, C.N., Rodriguez Presa, M.J., 2001. Sources, distribution and variability of airborne trace metals in La Plata City area, Argentina. *Environ. Pollut.* 111, 149–158.
- Bowie, A.R., Townsend, A.T., Lannuzel, D., Remenyi, T.A., van der Merwe, P., 2010. Modern sampling and analytical methods for the determination of trace elements in marine particulate material using magnetic sector inductively coupled plasma–mass spectrometry. *Anal. Chim. Acta* 676, 15–27.
- Cai, Q.-L., Dai, X.-R., Li, J.-R., Tong, L., Hui, Y., Cao, M.-Y., et al., 2020. The characteristics and mixing states of PM_{2.5} during a winter dust storm in Ningbo of the Yangtze River Delta, China. *Sci. Total Environ.* 709, 136146.
- Cesari, D., De Benedetto, G.E., Bonasoni, P., Busetto, M., Dinoi, A., Merico, E., et al., 2018. Seasonal variability of PM_{2.5} and PM₁₀ composition and sources in an urban background site in southern Italy. *Sci. Total Environ.* 612, 202–213.
- Chan, C.K., Yao, X., 2008. Air pollution in mega cities in China. *Atmos. Environ.* 42, 1–42.
- Cheng, Y., He, K.-B., Du, Z.-Y., Zheng, M., Duan, F.-K., Ma, Y.-L., 2015. Humidity plays an important role in the PM_{2.5} pollution in Beijing. *Environ. Pollut.* 197, 68–75.
- Chooabari, O.A., Zawar-Reza, P., Sturman, A., 2014. The global distribution of mineral dust and its impacts on the climate system: a review. *Atmos. Res.* 138, 152–165.
- Contini, D., Genga, A., Cesari, D., Siciliano, M., Donato, A., Bove, M.C., et al., 2010. Characterisation and source apportionment of PM₁₀ in an urban background site in Lecce. *Atmos. Res.* 95, 40–54.
- Cwiertny, David, Young, M., Mark, A., 2008. Chemistry and photochemistry of mineral dust aerosol. *Annu. Rev. Phys. Chem.* 59, 27–51.
- Dimitriou, K., Grivas, G., Liakakou, E., Gerasopoulos, E., Mihalopoulos, N., 2020. Assessing the contribution of regional sources to urban air pollution by applying 3D-PSCF modeling. *Atmos. Res.* 248, 105187.
- Dong, Z., Su, F., Zhang, Z., Wang, S., 2020. Observation of chemical components of PM_{2.5} and secondary inorganic aerosol formation during haze and sandy haze days in Zhengzhou, China. *J. Environ. Sci.* 88, 316–325.
- Draxler, R., Rolph, G., 2010. HYSPLIT (Hybrid Single-Particle Lagrangian Integrated Trajectory) model access via NOAA ARL READY website. 25. NOAA Air Resources Laboratory, Silver Spring, MD. <http://ready.arl.noaa.gov/HYSPLIT.php>.
- Du, W., Dada, L., Zhao, J., Chen, X., Daellenbach, K.R., Xie, C., et al., 2021. A 3D study on the amplification of regional haze and particle growth by local emissions. *npj Clim. Atmos. Sci.* 4, 1–8.

- Emberson, L.D., Ashmore, M.R., Murray, F., Kuylenstierna, J., Percy, K.E., Izuta, T., et al., 2001. Impacts of air pollutants on vegetation in developing countries. *Water Air Soil Pollut.* 130, 107–118.
- Fergusson, J.E., Kim, N.D., 1991. Trace elements in street and house dusts: sources and speciation. *Sci. Total Environ.* 100, 125–150.
- Font, A., Tremper, A.H., Priestman, M., Kelly, F.J., Canonaco, F., Prévôt, A.S.H., et al., 2022. Source attribution and quantification of atmospheric nickel concentrations in an industrial area in the United Kingdom (UK). *Environ. Pollut.* 293, 118432.
- Fu, X., Wang, S., Cheng, Z., Xing, J., Zhao, B., Wang, J., et al., 2014. Source, transport and impacts of a heavy dust event in the Yangtze River Delta, China, in 2011. *Atmos. Chem. Phys.* 14, 1239–1254.
- Fuzzi, S., Baltensperger, U., Carslaw, K., Decesari, S., Facchini, M.C., Denier, V.D.G.H., 2017. Particulate matter, air quality and climate: lessons learned and future needs. *Atmos. Chem. Phys.* 15, 8217–8299.
- Guan, Q., Cai, A., Wang, F., Yang, L., Xu, C., Liu, Z., 2017. Spatio-temporal variability of particulate matter in the key part of Gansu Province, Western China. *Environ. Pollut.* 230, 189–198.
- Gupta, D., Kim, H., Park, G., Li, X., Eom, H.J., Ro, C.U., 2015. Hygroscopic properties of NaCl and NaNO₃ mixture particles as reacted inorganic sea-salt aerosol surrogates. *Atmos. Chem. Phys.* 15, 3379–3393.
- Han, L., Zhuang, G., Cheng, S., Wang, Y., Li, J., 2007. Characteristics of re-suspended road dust and its impact on the atmospheric environment in Beijing. *Atmos. Environ.* 41, 7485–7499.
- Hao, Y., Guo, Z., Yang, Z., Ming, F., Feng, J., 2007. Seasonal variations and sources of various elements in the atmospheric aerosols in Qingdao, China. *Atmos. Res.* 85, 27–37.
- He, K., Zhao, Q., Ma, Y., Duan, F., Yang, F., Shi, Z., et al., 2012. Spatial and seasonal variability of PM_{2.5} acidity at two Chinese megacities: insights into the formation of secondary inorganic aerosols. *Atmos. Chem. Phys.* 12, 1377–1395.
- Hersbach, H., Bell, B., Berrisford, P., Hirahara, S., Horányi, A., Muñoz-Sabater, J., et al., 2020. The ERA5 global reanalysis. *Q. J. R. Meteorol. Soc.* 146, 1999–2049.
- Hu, J., Ying, Q., Wang, Y., Zhang, H., 2015. Characterizing multi-pollutant air pollution in China: comparison of three air quality indices. *Environ. Int.* 84, 17–25.
- Huang, L., Zhao, Y., Li, H., Chen, Z., 2015. Kinetics of heterogeneous reaction of sulfur dioxide on authentic mineral dust: effects of relative humidity and hydrogen peroxide. *Environ. Sci. Technol.* 49, 10797.
- Huang, X., Zhang, J., Luo, B., Wang, L., Tang, G., Liu, Z., et al., 2018. Water-soluble ions in PM_{2.5} during spring haze and dust periods in Chengdu, China: variations, nitrate formation and potential source areas. *Environ. Pollut.* 243, 1740–1749.
- Ke, L., Liu, W., Wang, Y., Russell, A.G., Edgerton, E.S., Zheng, M., 2008. Comparison of PM_{2.5} source apportionment using positive matrix factorization and molecular marker-based chemical mass balance. *Sci. Total Environ.* 394, 290–302.
- Ko, H.-J., Song, J.-M., Cha, J.W., Kim, J., Ryou, S.-B., Kang, C.-H., 2016. Chemical composition characteristics of atmospheric aerosols in relation to haze, Asian dust and mixed haze-Asian dust episodes at Gosan site in 2013. *J. Korea. Soc. Atmos. Environ.* 32, 289–304.
- Koçak, M., Theodosi, C., Zampas, P., Im, U., Bougiatioti, A., Yenigun, O., et al., 2011. Particulate matter (PM₁₀) in Istanbul: origin, source areas and potential impact on surrounding regions. *Atmos. Environ.* 45, 6891–6900.
- Kong, L., Tan, Q., Feng, M., Qu, Y., Wang, Z., 2019. Investigating the characteristics and source analyses of PM_{2.5} seasonal variations in Chengdu, Southwest China. *Chemosphere* 243, 125267.
- Kong, L., Feng, M., Liu, Y., Zhang, Y., Zhang, C., Li, C., et al., 2020. Elucidating the pollution characteristics of nitrate, sulfate and ammonium in PM_{2.5} in Chengdu, southwest China, based on 3-year measurements. *Atmos. Chem. Phys.* 20, 11181–11199.
- Kulshrestha, U.C., Raman, R.S., Kulshrestha, M.J., Rao, T.N., Hazarika, P.J., 2009. Secondary aerosol formation and identification of regional source locations by PSCF analysis in the Indo-Gangetic region of India. *J. Atmos. Chem.* 63, 33–47.
- Lee, B.-K., Hieu, N.T., 2011. Seasonal variation and sources of heavy metals in atmospheric aerosols in a residential area of Ulsan, Korea. *Aerosol Air Qual. Res.* 11, 679–688.
- Lee, S., Liu, W., Wang, Y., Armistead, G., Russell, E.S., et al., 2008. Source apportionment of PM_{2.5}: Comparing PMF and CMB results for four ambient monitoring sites in the southeastern United States. *Atmos. Environ.* 42, 4126–4137.
- Li, J., 2004. Transfer Mechanism of Heavy Metals During MSW Incineration and Solidification/Stabilization Technology of Heavy Metals in MSW Fly Ash. Zhejiang University Ph.D. Thesis.
- Li, X., Wang, S., Duan, L., Hao, J., Li, C., Chen, Y., et al., 2007. Particulate and trace gas emissions from open burning of wheat straw and corn stover in China. *Environ. Sci. Technol.* 41, 6052.
- Li, L., Yan, D., Xu, S., Huang, M., Wang, X., Xie, S., 2017. Characteristics and source distribution of air pollution in winter in Qingdao, eastern China. *Environ. Pollut.* 224, 44–53.
- Li, W., Wang, W., Zhou, Y., Ma, Y., Zhang, D., Sheng, L., 2018. Occurrence and reverse transport of severe dust storms associated with synoptic weather in East Asia. *Atmosphere* 10, 4.
- Li, X., Jin, L., Kan, H., 2019. Air pollution: a global problem needs local fixes. *Nature* 570, 437–439.
- Li, J., Zhang, Y., Cao, F., Zhang, W., Michalski, G., 2020. Stable sulfur isotopes revealed a major role of transition-metal-ion catalyzed SO₂ oxidation in haze episodes. *Environ. Sci. Technol.* 54, 2626–2634.
- Lin, C.-C., Chen, S.-J., Huang, K.-L., Lee, W.-J., Lin, W.-Y., Liao, C.-J., et al., 2007. Water-soluble ions in nano-ultrafine/fine/coarse particles collected near a busy road and at a rural site. *Environ. Pollut.* 145, 562–570.
- Lin, Y.C., Tsai, C.J., Wu, Y.C., Zhang, R., Chi, K.H., Huang, Y.T., et al., 2015. Characteristics of trace metals in traffic-derived particles in Hsuehshan tunnel, Taiwan: size distribution, potential source, and fingerprinting metal ratio. *Atmos. Chem. Phys.* 15, 4117–4130.
- Liu, T., Abbatt, J.P., 2021. Oxidation of sulfur dioxide by nitrogen dioxide accelerated at the interface of deliquesced aerosol particles. *Nat. Chem.* 13, 1173–1177.
- Liu, B., Song, N., Dai, Q., Mei, R., Sui, B., Bi, X., et al., 2016. Chemical composition and source apportionment of ambient PM_{2.5} during the non-heating period in Taian, China. *Atmos. Res.* 170, 23–33.
- Liu, B., Wu, J., Zhang, J., Wang, L., Yang, J., Liang, D., et al., 2017. Characterization and source apportionment of PM_{2.5} based on error estimation from EPA PMF 5.0 model at a medium city in China. *Environ. Pollut.* 222, 10–22.
- Liu, B., Sun, X., Zhang, J., Bi, X., Feng, Y., 2019. Characterization and spatial source apportionments of ambient PM₁₀ and PM_{2.5} during the heating period in Tianjin, China. *Aerosol Air Qual. Res.* 20, 1–13.
- Lucarelli, F., Barrera, V., Becagli, S., Chiari, M., Giannoni, M., Nava, S., et al., 2019. Combined use of daily and hourly data sets for the source apportionment of particulate matter near a waste incinerator plant. *Environ. Pollut.* 247, 802–811.
- Mace, Kimberly A., 2003. Organic nitrogen in rain and aerosol in the eastern Mediterranean atmosphere: an association with aerosol transport. *J. Geophys. Res.-Atmos.* 108.
- Marcazzan, G.M., Vaccaro, S., Valli, G., Vecchi, R., 2001. Characterisation of PM₁₀ and PM_{2.5} particulate matter in the ambient air of Milan (Italy). *Atmos. Environ.* 35, 4639–4650.
- McGowan, H., Clark, A., 2008. Identification of dust transport pathways from Lake Eyre Australia using Hysplit. *Atmos. Environ.* 42, 6915–6925.
- Morishita, M., Keeler, G.J., Kamal, A.S., Wagner, J.G., Harkema, J.R., Rohr, A., 2011. Identification of ambient PM_{2.5} sources and analysis of pollution episodes in Detroit, Michigan using highly time-resolved measurements. *Atmos. Environ.* 45, 1627–1637.
- Murano, K., Mukai, H., Hatakeyama, S., Oishi, O., Utsunomiya, A., Shimohara, T., 1998. Wet deposition of ammonium and atmospheric distribution of ammonia and particulate ammonium in Japan. *Environ. Pollut.* 102, 321–326.
- Nie, W., Wang, T., Xue, L.K., Ding, A.J., Wang, X.F., Gao, X.M., et al., 2012. Asian dust storm observed at a rural mountain site in southern China: chemical evolution and heterogeneous photochemistry. *Atmos. Chem. Phys.* 12, 11985–11995.
- Nie, W., Ding, A., Wang, T., Kerminen, V.-M., George, C., Xue, L., et al., 2014. Polluted dust promotes new particle formation and growth. *Sci. Rep.* 4, 6634.
- Odufer, F., Calvo, A.I., Blanco-Alegre, C., Castro, A., Nunes, T., Alves, C., et al., 2019. Unusual winter saharan dust intrusions at Northwest Spain: air quality, radiative and health impacts. *Sci. Total Environ.* 669, 213–228.
- Pan, X., Uno, I., Hara, Y., Kuribayashi, M., Kobayashi, H., Sugimoto, N., et al., 2015. Observation of the simultaneous transport of asian mineral dust aerosols with anthropogenic pollutants using a POPC during a long-lasting dust event in late spring 2014. *Geophys. Res. Lett.* 42, 1593–1598.
- Pandolfi, M., Gonzalez-Castanedo, Y., Alastuey, A., Rosa, J.D.D.L., Mantilla, E., Campa, A.S.D.L., et al., 2011. Source apportionment of PM₁₀ and PM_{2.5} at multiple sites in the strait of Gibraltar by PMF: impact of shipping emissions. *Environ. Sci. Pollut. Res.* 18, 260–269.
- Park, Y.-M., Park, K.-S., Kim, H., Yu, S.-M., Noh, S., Kim, M.-S., et al., 2018. Characterizing isotopic compositions of TC-C, NO₃ -N, and NH₄ -N in PM_{2.5} in South Korea: impact of China's winter heating. *Environ. Pollut.* 233, 735–744.
- Park, M.-B., Lee, T.-J., Lee, E.-S., Kim, D.-S., 2019. Enhancing source identification of hourly PM_{2.5} data in Seoul based on a dataset segmentation scheme by positive matrix factorization (PMF). *Atmos. Pollut. Res.* 10, 1042–1059.
- Pey, J., Pérez, N., Cortés, J., Alastuey, A., Querol, X., 2013. Chemical fingerprint and impact of shipping emissions over a western Mediterranean metropolis: primary and aged contributions. *Sci. Total Environ.* 463, 497–507.
- Pongkiatkul, P., Oanh, N.T.K., 2007. Assessment of potential long-range transport of particulate air pollution using trajectory modeling and monitoring data. *Atmos. Res.* 85, 3–17.
- Querol, X., Alastuey, A., Viana, M., Moreno, T., Reche, C., Minguillón, M.C., et al., 2013. Variability of carbonaceous aerosols in remote, rural, urban and industrial environments in Spain: implications for air quality policy. *Atmos. Chem. Phys.* 13, 6185–6206.
- Reff, A., Eberly, S.I., Bhawe, P.V., 2007. Receptor modeling of ambient particulate matter data using positive matrix factorization: review of existing methods. *J. Air Waste Manag. Assoc.* 57, 146–154.
- Ren, B., Xie, P., Xu, J., Li, A., Ji, H., 2021. Use of the PSCF method to analyze the variations of potential sources and transports of NO₂, SO₂, and HCHO observed by MAX-DOAS in Nanjing, China during 2019. *Sci. Total Environ.* 146865.
- Schauer, J.J., Kleeman, M.J., Cass, G.R., Simoneit, B.R.T., 2002. Measurement of emissions from air pollution sources. 5C1–C32 organic compounds from gasoline-powered motor vehicles. *Environ. Sci. Technol.* 36, 1169–1180.
- Shang, J., Khuzestani, R.B., Tian, J., Schauer, J.J., Hua, J., Zhang, Y., et al., 2019. Chemical characterization and source apportionment of PM_{2.5} personal exposure of two cohorts living in urban and suburban Beijing. *Environ. Pollut.* 246, 225–236.
- Shi, G.-L., Li, X., Feng, Y.-C., Wang, Y.-Q., Wu, J.-H., Li, J., et al., 2009. Combined source apportionment, using positive matrix factorization–chemical mass balance and principal component analysis/multiple linear regression–chemical mass balance models. *Atmos. Environ.* 43, 2929–2937.
- Shi, J., Guan, Y., Ito, A., Gao, H., Yao, X., Baker, A.R., et al., 2020. High production of soluble iron promoted by aerosol acidification in fog. *Geophys. Res. Lett.* 47, e2019GL086124.
- Soleimani, M., Amini, N., Sadeghian, B., Wang, D., Fang, L., 2018. Heavy metals and their source identification in particulate matter (PM_{2.5}) in Isfahan City/Iran. *J. Environ. Sci.* 72, 166–175.
- Sowlat, M.H., Hasheminassab, S., Sioutas, C., 2016. Source apportionment of ambient particle number concentrations in central Los Angeles using positive matrix factorization (PMF). *Atmos. Chem. Phys.* 16, 1–42.
- Tan, J., Duan, J., Zhen, N., He, K., Hao, J., 2015. Chemical characteristics and source of size-fractionated atmospheric particle in haze episode in Beijing. *Atmos. Res.* 167, 24–33.
- Tang, Y., Han, S., Yao, Q., Cai, Z., Feng, J., 2020. Analysis of a severe regional haze-fog-dust episode over North China in autumn by using multiple observation data. *Aerosol Air Qual. Res.* 20, 2211–2225.
- Tapper, P.U., 1993. Analysis of different modes of factor analysis as least squares fit problems. *Chemom. Intell. Lab. Syst.* 18, 183–194.

- Wang, Y., 2019. An open source software suite for multi-dimensional meteorological data computation and visualisation. *J. Open Res. Softw.* 7.
- Wang, G., Wang, H., Yu, Y., Gao, S., Feng, J., Gao, S., et al., 2003. Chemical characterization of water-soluble components of PM10 and PM2.5 atmospheric aerosols in five locations of Nanjing China. *Atmos. Environ.* 37, 2893–2902.
- Wang, X., Chen, J., Sun, J., Li, W., Yang, L., Wen, L., et al., 2014. Severe haze episodes and seriously polluted fog water in Ji'nan, China. *Sci. Total Environ.* 493, 133–137.
- Wang, M., Cao, C., Li, G., Singh, R.P., 2015. Analysis of a severe prolonged regional haze episode in the Yangtze River Delta China. *Atmos. Environ.* 102, 112–121.
- Wang, J., Liu, D., Ge, X., Wu, Y., Sun, Y., 2019. Characterization of black carbon-containing fine particles in Beijing during wintertime. *Atmos. Chem. Phys.* 19, 447–458.
- Wang, Z., Hu, W., Niu, H., Hu, W., Hu, M., 2020a. Variations in physicochemical properties of airborne particles during a heavy haze-to-dust episode in Beijing. *Sci. Total Environ.* 762, 143081.
- Wang, Z., Liu, C., Xie, Z., Hu, Q., Liu, J., 2020b. Elevated dust layers inhibit dissipation of heavy anthropogenic surface air pollution. *Atmos. Chem. Phys.* 20, 14917–14932.
- Wang, W., Liu, M., Wang, T., Song, Y., Ge, M., 2021. Sulfate formation is dominated by manganese-catalyzed oxidation of SO₂ on aerosol surfaces during haze events. *Nat. Commun.* 12, 1993.
- Wu, Y., Lin, S., Tian, H., Zhang, K., Wang, Y., Sun, B., et al., 2020. A quantitative assessment of atmospheric emissions and spatial distribution of trace elements from natural sources in China. *Environ. Pollut.* 259, 113918.
- Xiao, C., Li, S., Zhou, W., Shang, D., Zhao, S., Zhu, X., et al., 2013. The effect of air pollutants on the microecology of the respiratory tract of rats. *Environ. Toxicol. Pharmacol.* 36, 588–594.
- Xiao, J., Han, X., Sun, S., Wang, L., Rinklebe, J., 2021. Heavy metals in different moss species in alpine ecosystems of Mountain Gongga, China: geochemical characteristics and controlling factors. *Environ. Pollut.* 272, 115991.
- Yan, C., Zheng, M., Sullivan, A.P., Bosch, C., Desyatierik, Y., Andersson, A., et al., 2015. Chemical characteristics and light-absorbing property of water-soluble organic carbon in Beijing: biomass burning contributions. *Atmos. Environ.* 121, 4–12.
- Yang, Y.R., Liu, X.G., Qu, Y., An, J.L., Jiang, R., Zhang, Y.H., et al., 2015. Characteristics and formation mechanism of continuous hazes in China: a case study during the autumn of 2014 in the North China Plain. *Atmos. Chem. Phys.* 15, 10987–11029.
- Yang, S., Duan, F., Ma, Y., Li, H., He, K., 2019. Mixed and intensive haze pollution during the transition period between autumn and winter in BeijingChina. *Sci. Total Environ.* 711, 134745.
- Yang, S., Wang, Z., Huang, X., Wang, W., Sheng, L., Zhou, Y., 2021. Meteorological feedback and eco-environmental impact of asian dust: a simulation study. *Atmos. Environ.* 253, 118350.
- Yu, J.Z., Huang, X.-F., Xu, J., Hu, M., 2005. When aerosol sulfate goes up, so does oxalate: implication for the formation mechanisms of oxalate. *Environ. Sci. Technol.* 39, 128–133.
- Zeng, Y., Hopke, P.K., 1989. A study of the sources of acid precipitation in Ontario Canada. *Atmos. Environ.* 23, 1499–1509.
- Zhang, D., Iwasaka, Y., Shi, G., Zang, J., Matsuki, A., Trochline, D., 2003. Mixture state and size of Asian dust particles collected at southwestern Japan in spring 2000. *J. Geophys. Res.-Atmos.* 108.
- Zhang, Y.X., Sheesley, R.J., Schauer, J.J., Lewandowski, M., Jaoui, M., Nberg, Of Fe J.H., et al., 2009. Source apportionment of primary and secondary organic aerosols using positive matrix factorization (PMF) of molecular markers. *Atmos. Environ.* 43, 5567–5574.
- Zhang, X., Hecobian, A., Zheng, M., Frank, N.H., Weber, R.J., 2010. Biomass burning impact on PM_{2.5} over the southeastern US during 2007: integrating chemically speciated FRM filter measurements, MODIS fire counts and PMF analysis. *Atmos. Chem. Phys.* 10, 6839–6853.
- Zhang, Z.Y., Wong, M.S., Lee, K.H., 2015. Estimation of potential source regions of PM_{2.5} in Beijing using backward trajectories. *Atmos. Pollut. Res.* 6, 173–177.
- Zhang, Y., Wen, L., Chen, J., Wang, X., Xue, L., Yang, L., et al., 2018. Trend in fine sulfate concentrations and the associated secondary formation processes at an urban site in North China. *Aerosol Air Qual. Res.* 18, 1519–1530.
- Zhao, L., Wang, W., Hao, T., Qu, W., Zhou, Y., 2020a. The autumn haze-fog episode enhanced by the transport of dust aerosols in the Tianjin area. *Atmos. Environ.* 237, 117669.
- Zhao, Z.-Y., Cao, F., Fan, M.-Y., Zhang, W.-Q., Zhai, X.-Y., Wang, Q., et al., 2020b. Coal and biomass burning as major emissions of NO_x in Northeast China: implication from dual isotopes analysis of fine nitrate aerosols. *Atmos. Environ.* 242, 117762.
- Zhou, S., Yuan, Q., Li, W., Lu, Y., Zhang, Y., Wang, W., et al., 2014. Trace metals in atmospheric fine particles in one industrial urban city: spatial variations, sources, and health implications. *J. Environ. Sci.* 26, 205–213.
- Zong, Z., Wang, X., Tian, C., Chen, Y., Qu, L., Ji, L., et al., 2016. Source apportionment of PM_{2.5} at a regional background site in North China using PMF linked with radiocarbon analysis: insight into the contribution of biomass burning. *Atmos. Chem. Phys.* 16, 11249–11265.
- Zong, Z., Wang, X., Tian, C., Chen, Y., Fu, S., Qu, L., et al., 2018. PMF and PSCF based source apportionment of PM_{2.5} at a regional background site in North China. *Atmos. Res.* 203, 207–215.